Int. J. Electrochem. Sci., 16 **(2021)** Article ID: 21074, doi: 10.20964/2021.07.10

International Journal of
ELECTROCHEMICAL
SCIENCE
www.electrochemsci.org

Synthesis of Ag Nanoparticles Decorated Carbon Nanotubes as an Electrochemical Sensor for Determination of Phenolic Compounds in Shale Gas Wastewater

Yugao Zhu[1,*], *Lintao Yang*[2]

[1] Yan'an vocational and Technical College, Chemical engineering institute, Yanan, 716000, China
[2] Shenyang Research Institute of Chemical Industry Co. Ltd.
[*]E-mail:shanxi1850299@sina.com

Received: 4 March 2021/ *Accepted:* 13 April 2021 / *Published:* 31 May 2021

In this study, silver nanoparticles (Ag NPs) were decorated on carbon nanotubes (CNTs) for electrochemical determination of o-cresol and phenol as phenolic compounds in shale gas wastewater. The glassy carbon electrode (GCE) surface was modified with functionalized CNTs (CNTs/GCE) and Ag NPs were electrodeposited on CNTs/GCE (Ag NPs/CNTs/GCE). Morphology and structures analysis of synthesized electrodes were done using SEM and XRD which exhibited that the uniformly Ag NPs in fcc structure were electrodeposited on the side wall of CNTs. Electrochemical studies with cyclic voltammetry (CV), differential pulse voltammetry (DPV) and amperometry illustrated that there are stable and sensitive electrochemical signal for Ag NPs/CNTs/GCE due to enhancement of the surface area by synergetic effects of CNTs and Ag NPs. Electrochemical studies represented that the limit of detection, sensitivity and linear range of sensor were obtained 0.01 µM, 0.20046 µA/µM and 10 to 200 µM, respectively, for detection of o-cresol and 0.01 µM, 0.29759 µA/µM and 10 to 160 µM, respectively for determination of phenol. The selectivity and applicability of the sensor was considered to determine phenolic compounds in the prepared real sample of shale gas wastewater which implied the o-cresol concentration and phenol in the real sample were achieved 0.97 µM and 0.69 µM, respectively.

Keywords: Ag nanoparticles; Carbon nanotubes; Electrochemical sensor; Phenolic compounds; Shale gas wastewater

1. INTRODUCTION

Nowadays, shale gas has been an extendedly important source of natural gas in the world whose production shows the largest worldwide technological developments [1]. Extraction process causes large-scale air, soil and water pollution [2, 3]. The fracking industry as the main technology in gas extraction removes water from the water cycle and turns clean water into contaminated water which can return to the surface. Industry reports of shale gas exploration indicated that gas wells leak

which generate pathways for chemical migration and can lead to high levels of pollution in streams, aquifers and drinking water [4, 5]. Researchers have demonstrated that the exposure to toxic chemicals contaminated the environment lead to hormone disrupting, breathing difficulties, neurological impairment and cancer [6]. Moreover, evidence shows that animals and crops have been killed as a result of exposure to chemicals from fracking and drilling operations.

Phenolic compounds are increasingly used in the industry of resins, textile, nylons, plastics, rubber, antioxidants, oil additives, paper, drugs, pesticides, biocide, explosives, disinfectants and dyes [7-9]. These compounds consist of one or more hydroxyl groups which are directly connected to the basic aromatic Benzene ring. The various Phenolic compounds are formed by the substitution of one or more hydrogen atom on the Benzene ring by different atoms, molecules or carboxylic groups [10]. The most applicant phenolic compounds are including phenol, bisphenol A, butylated hydroxytoluene, 4-nonylphenol, orthophenylphenol, picric acid, phenolphthalein, xylenol, phenol-formaldehyde, resorcinol, catechol, hydroquinone, tyrosine, propofol and cresol. In addition, phenolic compounds have been observed among the oxygenated compounds present in petroleum that these generate deleterious effects for fuel quality and stability through formation of deposit and insoluble rubbers [11, 12]. Moreover, Phenol and its derivatives as hazardous material may present in wastewater of oil and gas industries.

Therefore, many studies have been conducted for determination of Phenolic compounds in wastewater and environments using gas chromatography, mass spectrometry, liquid chromatography, spectrophotometry, Folin-Ciocalteu assay, coulometry, flow injection and electrochemical techniques [13, 14]. Electrochemical techniques such as CV, DPV, linear sweep voltammetry (LSV), chronoamperometry and amperometry are interesting and developing determination techniques. A simple, low-cost and rapid strategy determination of phenolic compounds is achieved using modification of electrode surfaces. Modifying the electrode by one or more nanostructured materials enhances the chemical and physical properties of electrodes and promotes sensor efficiency [15-19]. Sensitivity and selectivity of sensors can enhance using nanomaterials because of increasing the effective surface area and electroactive sites on electrode surfaces [20-22]. Therefore, this study was carried out for synthesis of Ag NPs decorated CNTs as an electrochemical sensor for determination of phenolic compounds in shale gas wastewater.

2. EXPERIMENT

In order to modification the GCE with Ag NPs/CNTs, the GCE surface was polished with alumina slurry (99.6%, 0.2 μm, Dengfeng Sweet Abrasives Co., Ltd., China) for 20 minutes and rinsed with deionized (DI) water. The polished GCE was activated using cyclic voltammetry (CV) technique in an electrochemical cell in applied potential range of -1.5V to 1.5 V at scan rate of 20 mV/s in 0.1 M phosphate buffer solution (PBS) (pH 3) for 5 minutes. 0.1 g MWCNTs (diameter of 20-40 nm, length of 10-30 μm, XingtaiShineway Corporation Co., Ltd., China) were functionalized by oxidative treatments with mixture of 1 M aqueous mixture of H_2SO_4 (98%, Qingdao HiseaChem Co., Ltd., China) and HNO_3 (68%, Qingdao HiseaChem Co., Ltd., China) in volume ratio of 3:1 (v:v). The

MWCNTs were ultrasonically dispersed in a mixture solution for 5 minutes, and rinsed with DI water and ethanol (99.9%, Henan Sinowin Chemical Industry Co., Ltd.., China), respectively. The functionalized MWCNTs were ultrasonically dispersed in 0.4 µl dimethylformamide (DMF, >99%, Hebei Guanlang Biotechnology Co., Ltd., China) solution. The suspension was dropped onto the activated GCE surface. The GCE was transferred to an oven 70 °C and dried for 60 minutes. After electrode cooling, the electrode was immersed in electrochemical and Ag NPs were electrodeposited on MWCNTs/GCE from mixture of 0.5 mM $AgNO_3$ (99%, Merck) and 1M ascorbic acid (99%, Sigma-Aldrich) in 0.1 M phosphate buffer solutions (PBS) under applied potential range from -0.7 V to 1.4 V at scan rate of 20 mV/s for 7 minutes. The Ag NPs/MWCNTs/GCE was washed with DI water and dried at room temperature.

The scanning electron microscopy (SEM; JSM-6490LV, JEOL, Tokyo, Japan) and X-ray diffraction (XRD, Bruker, AXS, Karlsruhe, Germany) were applied to evaluate morphology and structures of synthesized electrodes. CV, DPV and amperometry measurements and electrodeposition were performed on AUTOLAB electrochemical system by three-electrode electrochemical cells containing Ag/AgCl, Pt wire and the prepared electrodes as reference, counter and working electrodes, respectively. 0.1M PBS as electrochemical electrolyte was produced by 0.1M H_3PO_4 and 0.1M NaH_2PO_4.

For study the real sample, the wastewater used in this study was taken from a shale gas field located in the Eastern Sichuan Basin in China. The wastewater was filtered and centrifuged at 1000 rpm. The resulting supernatant was used to prepare of 0.1 PBS.

3. RESULTS AND DISCUSSION

Structure of powder of prepared CNTs, Ag NPs and Ag NPs/CNTs were examined using the XRD analysis. Figure 2a shows a strong single diffraction peak at 26.18° corresponding to the (002) plane of graphite structure in CNTs (JCPDS card no. 75-1621).

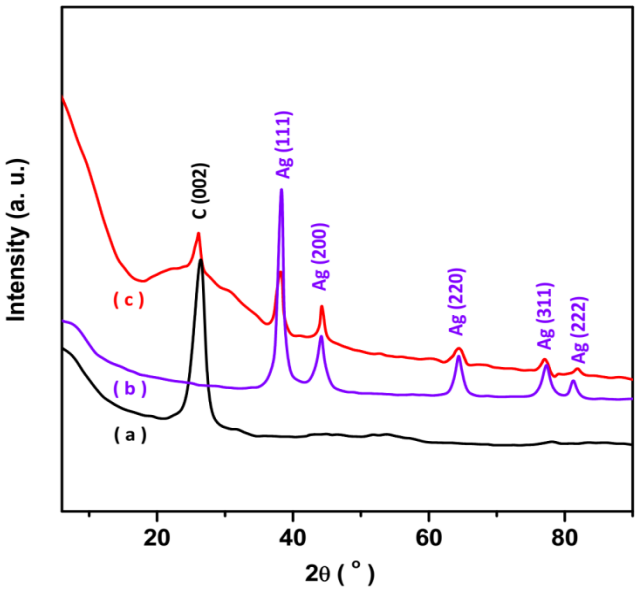

Figure 1. XRD patterns of powder of (a) CNTs, (b) Ag NPs and (c) Ag NPs/CNTs.

The XRD pattern of Ag NPs reveals the diffraction peaks at 38.14°, 44.21°, 64.70°, 77.39° and 81.38° that indicated to formation of (111), (200), (220), (311) and (222) crystalline planes of Ag in fcc structure (JCPDS no. 04-0783), respectively. The XRD pattern of Ag NPs/CNTs displays the both of CNTs and Ag NPs diffraction peaks which implied to effectively anchoring of Ag NPs on CNTs surface.

The SEM images of CNTs/GCE and Ag NPs/CNTs/GCE are shown in Figure 2. As observed from Figure 2a, there are functionalized CNTs in diameter of 90 nm and length of 3 µm. The SEM image of Ag NPs/CNTs/GCE in Figure 2b shows the uniform distribution of Ag NPs on the side wall of CNTs. Functionalization of CNTs in H_2SO_4 and HNO_3 cause to cut highly tangled long fiber of CNTs into shorter open-ended pipes and form many carboxylic and oxygen-containing groups at the open end [23]. Oxygen functional groups such as on hydroxyl, epoxy and carboxylic groups on the both basal plane and edge of CNTs act as anchoring sites for Ag NPs [24].

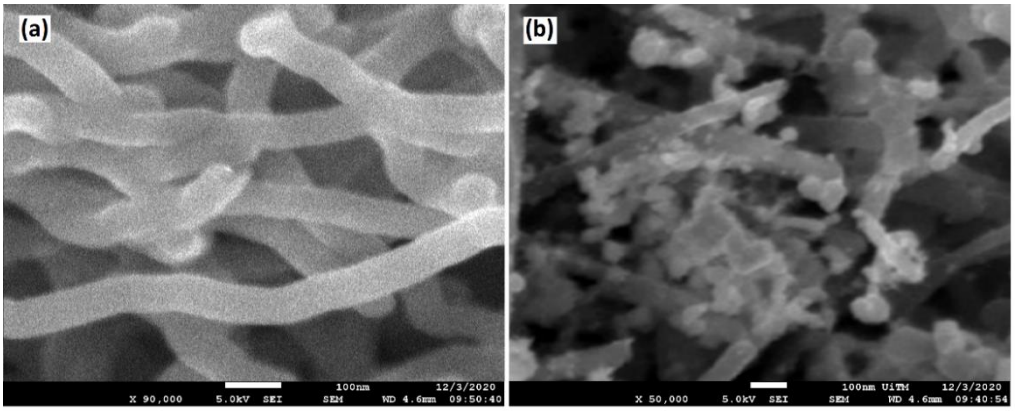

Figure 2. SEM images of (a) CNTs, and (b) Ag NPs/CNTs.

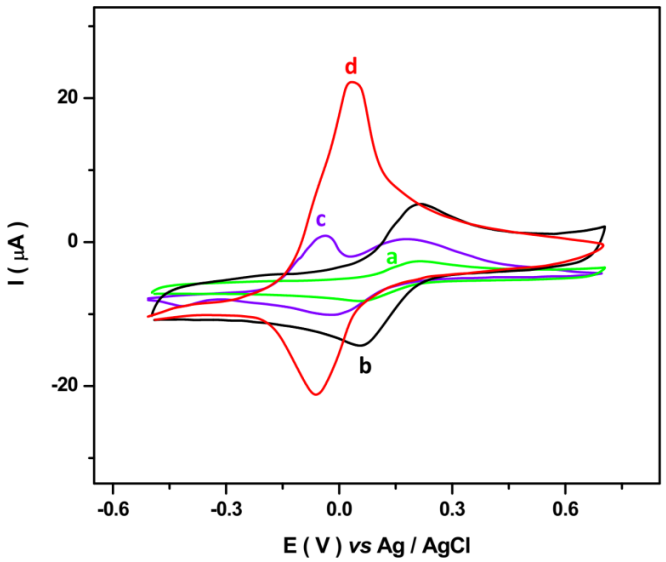

Figure 3. The electrochemical responses of (a) GCE, (b) CNTs/GCE, (c) Ag NPs/GCE and (d) Ag NPs/CNTs/GCE using CV measurements in 0.1M PBS (pH: 6.5) including 0.1M KCl and 5mM $[Fe(CN)6]^{3-/4-}$ at 20 mV/s scan rate.

The electrochemical properties of GCE, CNTs/GCE, Ag NPs/GCE and Ag NPs/CNTs/GCE were studied using CV measurements in 0.1M PBS (pH: 6.5) including 0.1M KCl and 5mM $[Fe(CN)6]^{3-/4-}$ as redox-active material at 20 mV/s scan rate. As observed, there are the $[Fe(CN)6]^{3-/4-}$ reversible one-electron redox at 0.20 V and 0.05 V on the recorded CVs of GCE and CNTs/GCE that those are exhibiting the reduction of Fe^{3+} to Fe^{2+} of$[Fe(CN)6]^{3-/4-}$ solution [25].

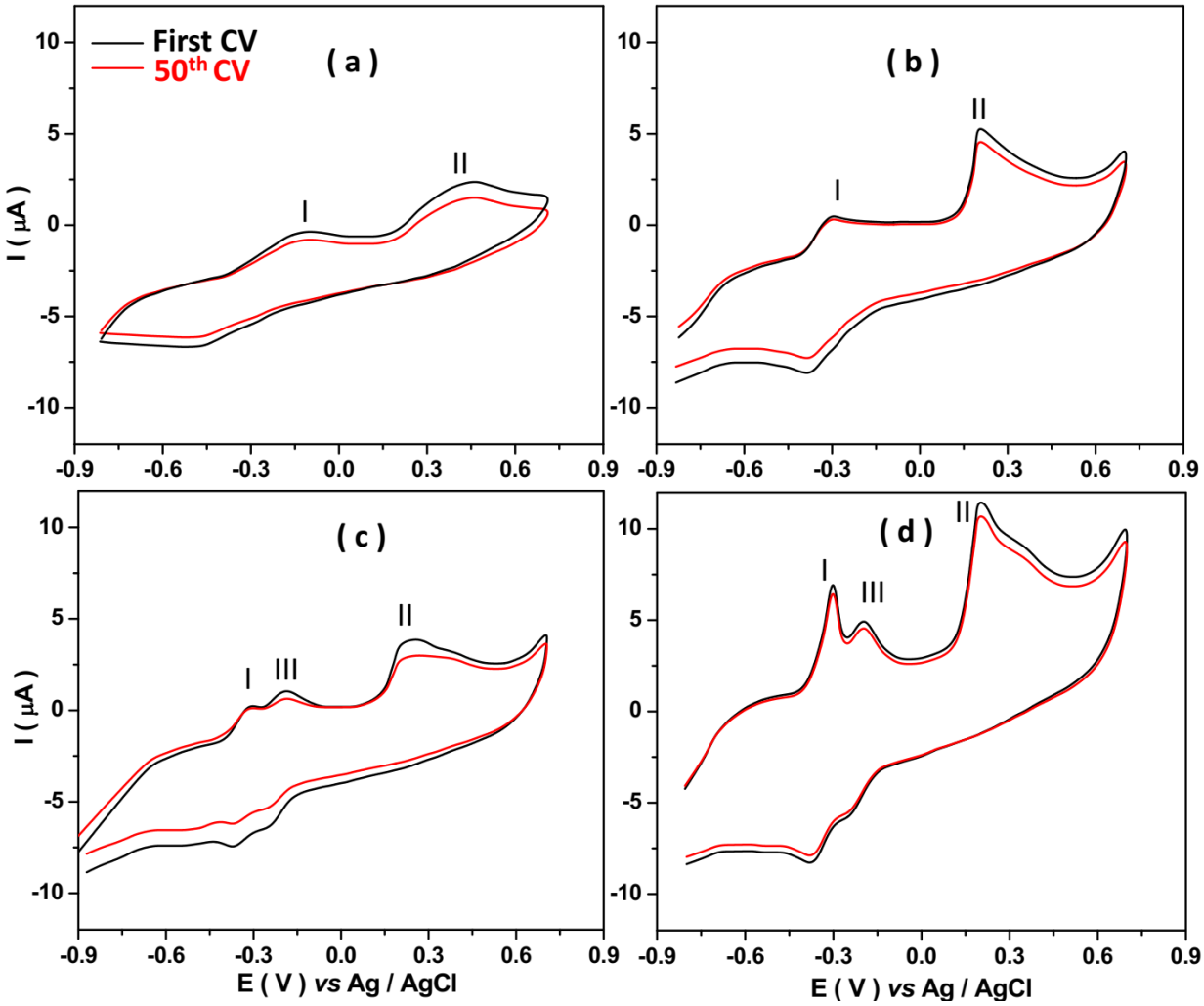

Figure 4. The first and 50th electrochemical responses of (a) GCE, (b) CNTs/GCE, (c) Ag NPs/GCE and (d) Ag NPs/CNTs/GCE using CV in 0.1M PBS (pH: 6.5) including 10 µM o-cresol and 10 µM phenol solutions at scan rate of 20 mV/s.

The electrochemical current response of CNTs/GCE is higher than GCE because of large effective surface area and higher conductivity of CNTs [26]. The recorded CV of Ag NPs/GCE displays a strong oxidation and reduction peaks at -0.04 V and −0.41 V, respectively, which correlated with the electrochemical reduction of Ag^{+} to Ag^{0} during first cathodic sweep and re-oxidation Ag^{0} to Ag^{+} during first anodic sweep [27], and demonstrated to successfully electrodeposition of Ag NPs on surface of GCE. Moreover, the redox peaks -0.17 V and −0.01 V are indicated to the redox activity of $[Fe(CN)6]^{3-/4-}$. For Ag NPs/CNTs/GCE, the recorded CV exhibits the peak current enhanced 4.9 and 6.3 times higher than the recorded peak current of CNTs/GCE and Ag NPs/GCE, respectively, that it

attributed to increase the surface area of the electrode by simultaneous effects of CNTs and Ag NPs [28, 29]. In addition, the redox peaks of both Ag^0/Ag^+ and $[Fe(CN)6]^{3-/4-}$ be revealed in the close potential range and the recorded CV of Ag NPs/CNTs/GCE shows the sum of the electrochemical responses of them at 0.40 V and -0.06 V. Therefore, results evidently represent that Ag NPs/CNTs/GCE has been strongly electrodeposited on GCE.

Figure 4 depicts the recorded CV responses of GCE, CNTs/GCE, Ag NPs/GCE and Ag NPs/CNTs/GCE in 0.1M PBS (pH: 6.5) including 10 µM o-cresol and 10 µM phenol solutions at scan rate of 20 mV/s. For GCE (Figure 4a), two low intensity redox peaks appear at potential of -0.14 V (I) and 0.43 V (II) which are related to oxidation of o-cresol and phenol, respectively. In Figure 4b, the CNTs/GCE shows these peaks obviously at -0.29 V and 0.20 V. CV of Ag NPs/GCE in Figure 4c exhibits the similar responses to unmodified GCE and characteristic oxidation peak of Ag^0/Ag^+ is observed at potential of -0.18 V (III). The recorded CV of Ag NPs/CNTs/GCE not only shows the similar responses to Ag NPs/GCE but also separated and higher current of oxidation peaks for phenolic compounds which implied to attachment of Ag NPs on CNTs walls provide the fast transport path for electrons and can enhance the resolution of oxidation peaks of phenolic compounds [30]. Moreover, the different potential for oxidation of analytes leads to selective responses of all electrode surfaces to simultaneous determination of the two phenolic compounds. Therefore, the advantages from the synergistic effect between the good electron transfer efficiency of AgNPs and easy functionalization of CNTs in Ag NPs/CNTs/GCE represents great electrocatalytic activity for simultaneous determination of the phenolic compounds [31].

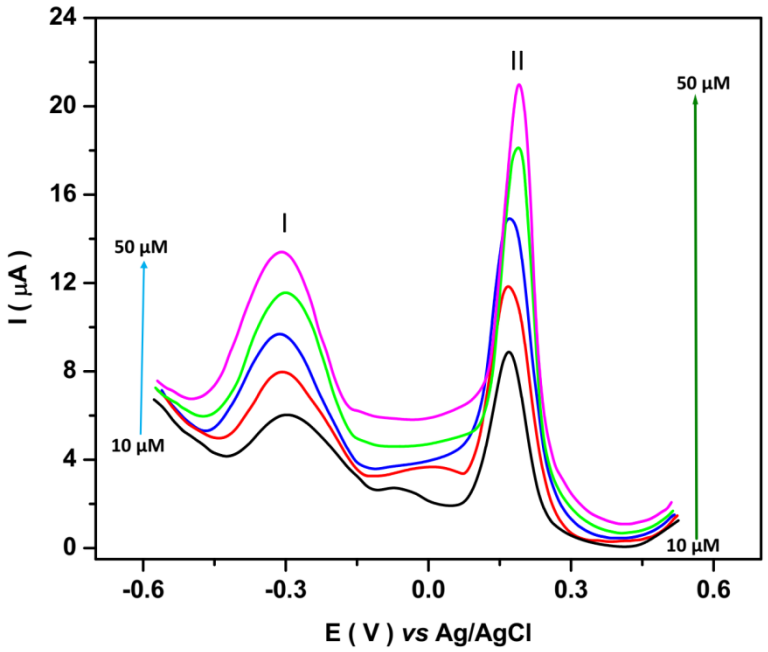

Figure 5. The concentration effect of o-cresol (10 to 50 µM) and phenol (10 to 50 µM) on elctrocatalytic response of Ag NPs/CNTs/GCE in 0.1M PBS (pH: 6.5) at 20 mV/s scan rate.

The stability of electrocatalytic responses of all electrodes were also investigated in 0.1M PBS (pH: 6.5) including 10 µM o-cresol and 10 µM phenol solutions at scan rate of 20 mV/s. As seen in

Figure 4, the reduction of the first and 50th recorded peak currents of o-cresol and phenol for GCE, CNTs/GCE, Ag NPs/GCE and Ag NPs/CNTs/GCE are 35%, 11%, 21% and 8%, respectively. The lowest change in electrochemical response signifies a higher stability response of electrodes to simultaneous determination of these phenolic compounds. Thus, the following electrochemical measurements were carried out with Ag NPs/CNTs/GCE.

The DPV study was conducted on the concentration effect of o-cresol and phenol on electrocatalytic response of Ag NPs/CNTs/GCE in 0.1 M PBS pH 6.5 at scan rate of 20 mV/s. As observed from Figure 5, the recorded CVs in simultaneous successive injections of 10 µM o-cresol and 10 µM phenol solutions display that the oxidation peaks are linearly increased with increasing the o-cresol (peak I) and phenol (peak II) concentrations.

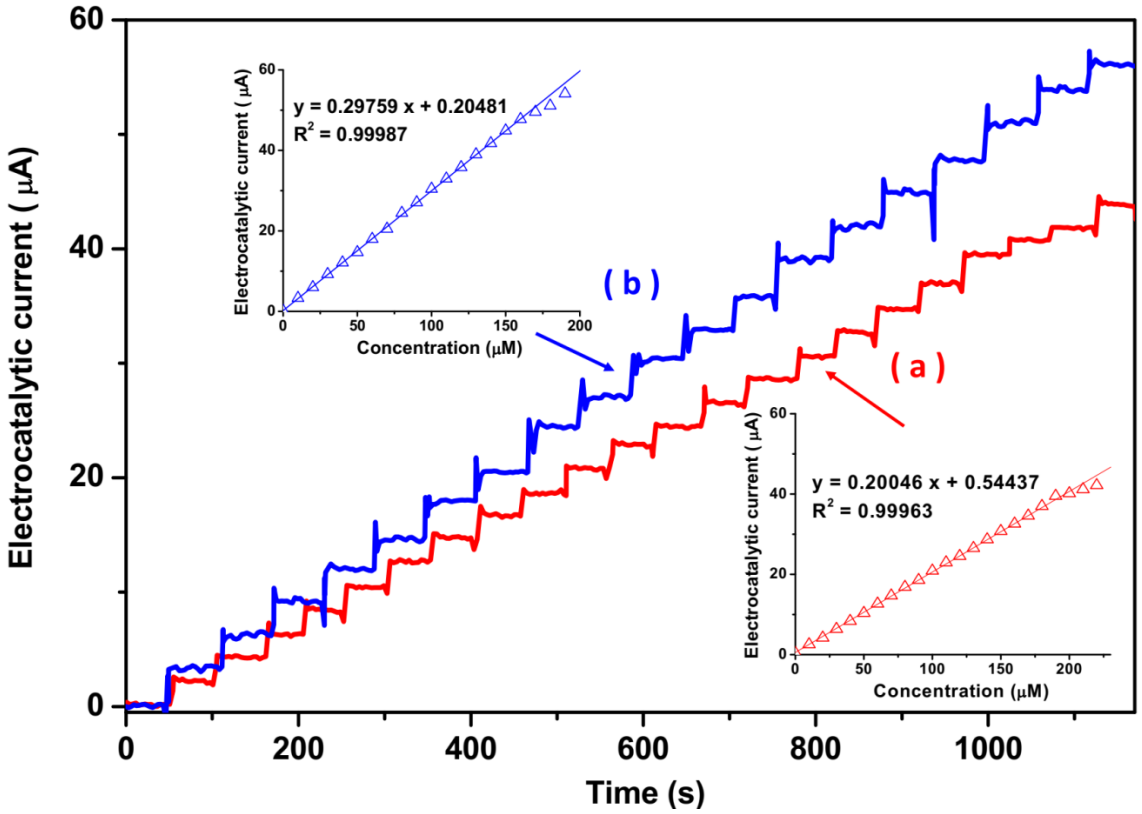

Figures 6. The amperomerty responses and the calibration plots of Ag NPs/CNTs/GCE in 0.1M PBS (pH: 6.5) for separated successive addition of (a) 10 µM o-cresol (applied potential at -0.3 V) and (b) 10 µM phenol (applied potential at 0.2 V) solutions.

Further studies were performed using the amperometry method to obtain the limit of detection, sensitivity and linear range of o-cresol and phenol with Ag NPs/CNTs/GCE sensor. Figure 6a and 6b shows the ampermerty responses and the calibration plots of Ag NPs/CNTs/GCE in 0.1M PBS (pH: 6.5) for separated successive addition of 1 µM o-cresol (applied potential at -0.3 V) and 1 µM phenol (applied potential at 0.2 V) solutions. Both of the recorded amperograms illustrate the fast response of sensors toward successive addition of the phenolic compounds. The current responses are improved linearly by addition of both of analytes. The limit of detection, sensitivity and linear range of sensor

are obtained 0.01 µM, 0.20046 µA/µM and 10 to 200 µM, respectively, for determination of o-cresol and 0.01 µM, 0.29759 µA/µM and 10 to 160 µM, respectively for determination of phenol. Table 1 shows the comparison between the achieved sensing values of Ag NPs/CNTs/GCE and other reported these phenolic compounds sensors. It is represented to acceptable sensing properties of prepared sensors in this study than other sensors in Table 1. It is suggested functionalization of CNTs can increase the immobilization sites for electrodeposited Ag NPs and provide the high stable and promising candidate for o-cresol and phenol determinations [32].

Table 1. Comparison between achieved sensing values of Ag NPs/CNTs/GCE and other reported these phenolic compounds sensors.

Electrode	**phenolic compound**	**Technique**	**Linear Range (µM)**	**limit of detection (µM)**	**Ref.**
Ag NPs/CNTs/GCE	o-cresol	ampermerty	10 to 200	0.010	This work
Ag NPs/CNTs/GCE	phenol	ampermerty	10 to 160	0.010	This work
ZnOnanosheets/screen printed electrode	phenol	LSV	0.01 to 50	0.0041	[17]
ZnOnanosheets/screen printed electrode	o-cresol	LSV	0.01 to 50	0.0055	[17]
Mesoporous silica/ carbon paste electrode	o-cresol	CV	10 to 500	0.9	[33]
activated carbon/ carbon paste electrode	o-cresol	CV	10 to 500	0.5	[33]
GCE	phenol	CV	0 to 100	11.25	[34]
GCE	o-cresol	CV	42 to 100	42.02	[34]
MWCNT/surfactant/tyrosinase/carbon paste electrode	phenol	CV	1.5 to 25	2.9	[35]
boron-doped diamond film	phenol	DPV	50 to 10000	1.8	[36]

The selectivity of the sensor was examined in present of some phenolic components such as nitrophenol, hydroquinone , catechol and bisphenol A and some metallic ion such as Co^{2+}, Pb^{2+}, Cd^{2+}, Co^{2+}, Cu^{2+}, Mg^{2+}, K^{+} and Li^{+} as interferents. Table 2 shows the obtained electrocatalytic current using amperometry technique on Ag NPs/CNTs/GCE in 0.1 M PBS pH 6.5 at -0.3 V for addition of 10 µM o-cresol and successive additions of 50 µM of interference. As observed, the prepared electrode demonstrates an obvious signal to additions of o-cresol solution and there are not significant signals for the additions of interference and phenol under applied potential at -0.3 V. Table 3 shows that the similar measurements were repeated for study the interference effect on phenol determination on Ag NPs/CNTs/GCE at 0.2 V for addition of 10 µM phenol and successive additions of 50 µM of interference. The results equally confirm the stability of the Ag NPs/CNTs/GCE representing that substance and o-cresol do not interfere with the surface of the electrode under applied potential at 0.2 V.

Table 2. The recorded electrocatalytic currents using amperometry technique on Ag NPs/CNTs/GCE in 0.1 M PBS pH 6.5 at -0.3 V for addition of 10 µM o-cresol and successive additions of 50 µM of interferents.

substance	**Added (µM)**	**Electrocatalytic current response (µA)**	**RSD (%)**
O-cresol	10	2.010	±0.012
Phenol	50	0.026	±0.008
Nitrophenol	50	0.027	±0.004
Hydroquinone	50	0.098	±0.011
Catechol	50	0.026	±0.005
Bisphenol A	50	0.031	±0.007
Co^{2+}	50	0.077	±0.009
Pb^{2+}	50	0.058	±0.004
Cd^{2+}	50	0.022	±0.004
Co^{2+}	50	0.038	±0.006
Cu^{2+}	50	0.025	±0.007
Mg^{2+}	50	0.023	±0.004
K^{+}	50	0.027	±0.004
Li^{+}	50	0.037	±0.007

Table 3. The recorded electrocatalytic currents using amperometry technique on Ag NPs/CNTs/GCE in 0.1 M PBS pH 6.5 at 0.2 V for addition of 10 µM phenol and successive additions of 50 µM of interferents.

substance	**Added (µM)**	**Electrocatalytic current response (µA)**	**RSD (%)**
Phenol	10	2.986	±0.018
O-cresol	50	0.066	±0.007
Nitrophenol	50	0.084	±0.010
Hydroquinone	50	0.048	±0.009
Catechol	50	0.021	±0.005
Bisphenol A	50	0.061	±0.007
Co^{2+}	50	0.035	±0.005
Pb^{2+}	50	0.033	±0.004
Cd^{2+}	50	0.034	±0.005
Co^{2+}	50	0.029	±0.007
Cu^{2+}	50	0.028	±0.006
Mg^{2+}	50	0.029	±0.004
K^{+}	50	0.034	±0.009
Li^{+}	50	0.041	±0.008

Applicability of the sensor was examined to detect phenolic compounds in prepared real samples of shale gas wastewater by amperometry measurements in pH 6.5. Figure 7a shows the recorded amperometric response and calibration curve of Ag NPs/CNTs/GCE in successive addition of 10 µM o-cresol solutions at -0.30 V which implied to the o-cresol concentration in prepared PBS of wastewater is obtained 0.97 µM. This measurements was repeated for successive addition of 10 µM phenol solutions at 0.2 V (Figure 7b) which indicated to the initial phenol content in shale gas wastewater is 0.69 µM.Moreover,the analytical applicability of the Ag NPs/CNTs/GCE was also evaluated to determine o-cresol and phenol in prepared real samples of shale gas wastewater. Table 4 shows the obtained recovery values more than 95.0% and 92.2% for o-cresol and phenol, respectively, and RSDvalues less than 4.87% and 4.91% for o-cresol and phenol, respectively. These results indicate the good accuracy of the proposed sensor to determine of phenolic compounds in shale gas wastewater.

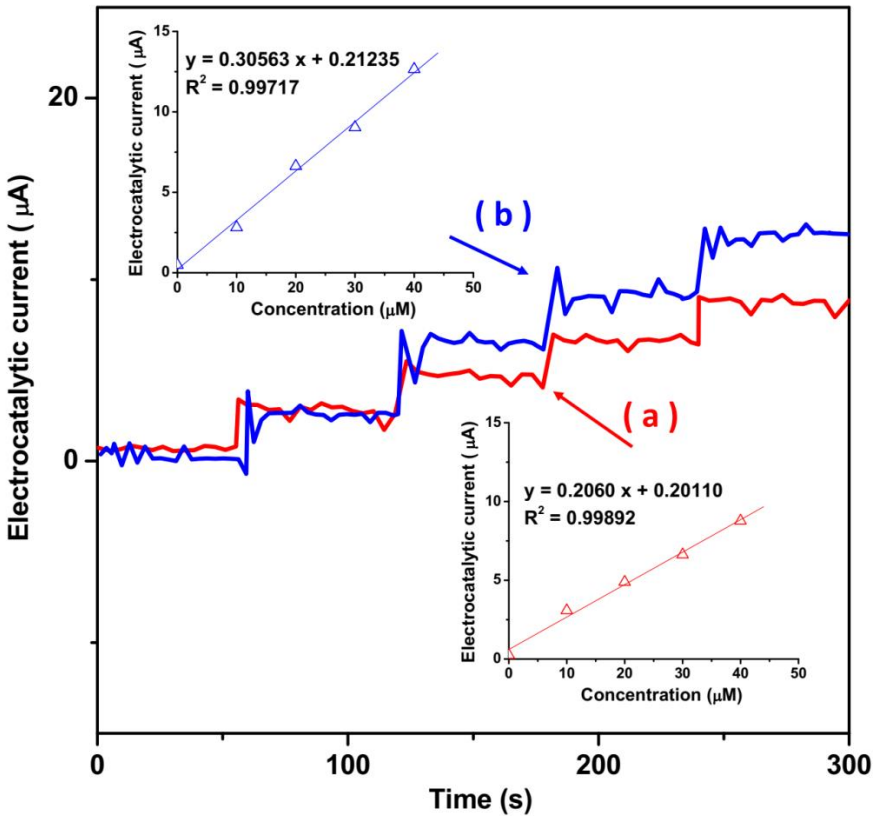

Figure 7. Recorded amperometric responses and calibration plots of Ag NPs/CNTs/GCE in prepared real sample of shale gas wastewater pH 6.5 at 1000 rpm rotating speed into the successive addition of (a) 10 µM o-cresol solutions at -0.3 V and (b) 10 µM phenol solutions at 0.2 V.

Table 4. The analytical results of determination of o-cresol and phenol in the prepared real sample of shale gas wastewater(n = 4).

Phenolic compounds	**Added (µM)**	**Found (µM)**	**Recovery (%)**	**RSD (%)**
o-cresol	10.0	9.5	95.0	3.10
	20.0	19.7	98.5	4.11
	30.0	28.9	96.3	3.75
	40.0	39.1	97.7	4.87
phenol	10.0	9.7	97.0	3.87
	20.0	19.6	98.0	2.87
	30.0	29.3	97.7	3.88
	40.0	39.7	99.2	4.91

4. CONCOUSION

This study was performed to synthesis of Ag NPs decorated CNTs for electrochemical determination of o-cresol and phenol as phenolic compounds in shale gas wastewater. The GCE surface was modified with functionalized MWCNTs and Ag NPs were electrodeposited on CNTs/GCE. Morphology and structures analysis of synthesized electrodes were done using SEM and XRD which exhibited that the uniformly Ag NPs in fcc structure were electrodeposited on the side wall of CNTs. Electrochemical studies showed that Ag NPs/CNTs/GCE had higher electrochemical signal than CNTs/GCE and Ag NPs/GCE due to enhancement of the surface area by synergetic effects of CNTs and Ag NPs. Electrochemical measurements displayed that the limit of detection, sensitivity and linear range of sensor were obtained 0.01 µM, 0.20046 µA/µM and 10 to 200 µM, respectively, for determination of o-cresol and 0.01 µM, 0.29759 µA/µM and 10 to 160 µM, respectively for determination of phenol. The selectivity sensor and applicability of the sensor was examined to detect phenolic compounds in prepared real samples of shale gas wastewater which implied the o-cresol concentration and phenol in real samples were achieved 0.97µM and 0.69µM, respectively.

ACKNOWLEDGEMENT
This work is carried out by the Yan'an 2020 science and Technology Program (topic 2019 zcgy-001).

References

1. J. Selivanovs, E. Vigants, V. Priedniece, I. Veidenbergs and D. Blumberga, *Energy Procedia*, 128 (2017) 379.
2. M. Chen, W. Lu, Z. Hou, Y. Zhang, X. Jiang and J. Wu, *Environmental Science and Pollution Research*, 24 (2017) 3084.

3. H. Karimi-Maleh, Y. Orooji, A. Ayati, S. Qanbari, B. Tanhaei, F. Karimi, M. Alizadeh, J. Rouhi, L. Fu and M. Sillanpää, *Journal of Molecular Liquids*, 329 (2021) 115062.
4. P.A. Hammond, T. Wen, S.L. Brantley and T. Engelder, *Hydrogeology Journal*, 28 (2020) 1481.
5. J. Rouhi, S. Kakooei, M.C. Ismail, R. Karimzadeh and M.R. Mahmood, *International Journal of Electrochemical Science*, 12 (2017) 9933.
6. D.R. Boyd and S.J. Genuis, *Environmental Research*, 106 (2008) 240.
7. X. Luo, H. Zheng, Z. Zhang, M. Wang, B. Yang, L. Huang and M. Wang, *Microchemical Journal*, 137 (2018) 148.
8. H. Karimi-Maleh, M.L. Yola, N. Atar, Y. Orooji, F. Karimi, P.S. Kumar, J. Rouhi and M. Baghayeri, *Journal of colloid and interface science*, 592 (2021) 174.
9. S. Kakooei, H.M. Akil, A. Dolati and J. Rouhi, *Construction and Building Materials*, 35 (2012) 564.
10. M. Mousavi and E.H. Fini, *Fuel*, 287 (2021) 119532.
11. M.A. Farajzadeh, A. Yadeghari, L. Khoshmaram and H. Ghorbanpour, *Journal of separation science*, 37 (2014) 2966.
12. H. Karimi-Maleh, M. Alizadeh, Y. Orooji, F. Karimi, M. Baghayeri, J. Rouhi, S. Tajik, H. Beitollahi, S. Agarwal and V.K. Gupta, *Industrial & Engineering Chemistry Research*, 60 (2021) 816.
13. C. Proestos, D. Sereli and M. Komaitis, *Food chemistry*, 95 (2006) 44.
14. M.L. Way, J.E. Jones, D.S. Nichols, R.G. Dambergs and N.D. Swarts, *Beverages*, 6 (2020) 55.
15. R. Savari, S. Soltanian, A. Noorbakhsh, A. Salimi, M. Najafi and P. Servati, *Sensors and Actuators B: Chemical*, 176 (2013) 335.
16. R. Savari, H. Savaloni, S. Abbasi and F. Placido, *Sensors and Actuators B: Chemical*, 266 (2018) 620.
17. J. Liu, H. Huang, S. Zhong, X. She and D. Yin, *International Journal of Electrochemical Science*, 11 (2016) 3921.
18. H. Savaloni, R. Savari and S. Abbasi, *Current Applied Physics*, 18 (2018) 869.
19. H. Karimi-Maleh, S. Ranjbari, B. Tanhaei, A. Ayati, Y. Orooji, M. Alizadeh, F. Karimi, S. Salmanpour, J. Rouhi and M. Sillanpää, *Environmental Research*, 195 (2021) 110809.
20. F. Liu, S. Dong, Z. Zhang, X. Dai, Y. Xin, X. Wang, K. Liu, Z. Yuan, J. Zhang and M. Chen, *International Journal of Electrochemical Science*, 14 (2019) 9122.
21. Z. Meng, M. Li, C. Li, X. Liu and Z. Lei, *International Journal of Electrochemical Science*, 14 (2019) 3126.
22. F. Chahshouri, H. Savaloni, E. Khani and R. Savari, *Journal of Micromechanics and Microengineering*, 30 (2020) 075001.
23. R. Yudianti, H. Onggo, Y. Saito, T. Iwata and J.-i. Azuma, *The Open Materials Science Journal*, 5 (2011) 242.
24. M. Song, J. Xu and C. Wu, *Journal of Nanotechnology*, 2012 (2012) 1.
25. E.E. Elemike, D.C. Onwudiwe, O.E. Fayemi and T.L. Botha, *Applied Physics A*, 125 (2019) 42.
26. S.E. Elugoke, A.S. Adekunle, O.E. Fayemi, B.B. Mamba, T.T. Nkambule, E.S.M. Sherif and E.E. Ebenso, *Nano Select*, 1 (2020) 561.
27. S. Dave, *Indian Journal of Chemical Technology (IJCT)*, 25 (2018) 201.
28. I.-H. Cho, D.H. Kim and S. Park, *Biomaterials research*, 24 (2020) 1.
29. L.A. Goulart, R. Gonçalves, A.A. Correa, E.C. Pereira and L.H. Mascaro, *Microchimica Acta*, 185 (2018) 1.
30. Y. Zhang, Z. Wang, Y. Ji, S. Liu and T. Zhang, *RSC Advances*, 5 (2015) 39037.
31. D. Xu, B. Hou, L. Qian, X. Zhang and G. Liu, *Molecules*, 24 (2019) 3411.

32. J.R. Rajabathar, G. Periyasamy, A.M. Alanazi, M. Govindasamy and P. Arunachalam, *Processes*, 8 (2020) 1654.
33. A. Białek, K. Skrzypczyńska, K. Kuśmierek and A. Świątkowski, *International Journal of Electrochemical Science*, 14 (2019) 228.
34. L. Fotouhi, M. Ganjavi and D. Nematollahi, *Sensors*, 4 (2004) 170.
35. S. Hashemnia, S. Khayatzadeh and M. Hashemnia, *Journal of Solid State Electrochemistry*, 16 (2012) 473.
36. G.H. ZHAO, Y.T. TANG, M.C. LIU, Y.Z. LEI and X.E. XIAO, *Chinese Journal of Chemistry*, 25 (2007) 1445.